PAPER

A novel energy absorber based on magnetorheological gel

IOP Publishing Smart Materials and Structures
Smart Mater. Struct. 26 (2017) 105017 (9pp) https://doi.org/10.1088/1361-665X/aa834c

A novel energy absorber based on magnetorheological gel

Haoming Pang, Shouhu Xuan, Chuanlin Sun and Xinglong Gong

CAS Key Laboratory of Mechanical Behavior and Design of Materials, Department of Modern Mechanics, University of Science and Technology of China (USTC), Hefei 230027, People's Republic of China

E-mail: gongxl@ustc.edu.cn

Received 19 May 2017, revised 15 July 2017
Accepted for publication 1 August 2017
Published 12 September 2017

Abstract

In this work, a novel magnetorheological energy absorber (MREA) was designed by using magnetorheological gel (MRG) as the damping medium. The proposed MREA had tunable piston gap distances and variable inner magnetic flux density distribution. The piston gap distance could be varied from 7–2 mm and the magnetic flux density at the gap increased from 120–860 mT, respectively. Under both low velocity compression and high speed impact, the damping could be divided into three parts. In the impact test, the velocity of a drop hammer could be reduced from to 3.4–0 m s^{-1} within a very short time (13 ms) and distance (17 mm). The maximum damping force of the MREA reached to as high as 8 kN. The damping force could also be adjusted by changing the current input. Under a 2 A current, the energy absorption ratio increased about 23% (from 4.13–5.07 J mm^{-1}).

Keywords: energy absorber, magnetorheological gels, structure design, tunable piston gap, impact

(Some figures may appear in colour only in the online journal)

Introduction

A traditional energy absorber (EA) is designed to dissipate impact energy and decrease injury, thus it has been widely applied in the railway industry and earthquake engineering [1, 2]. A magnetorheological energy absorber (MREA) is an adaptive energy absorber which can reversibly and rapidly adjust the damping force by changing the current input [3–7]. Different from the traditional passive energy absorber, the damping mediums in MREAs are magnetorheological (MR) materials whose mechanical properties are sensitive to the external magnetic field. To this end, the MREAs are advantageous in many areas that require precise control.

The MREA is a specific MR damper designed for absorbing impact energy. The damping medium in most of the previously reported MREAs was MR fluids [8–11]. MR fluids were usually prepared by dispersing micro-sized carbonyl iron particles into nonmagnetic fluids. Under applying a magnetic field, the yield stress of the MR fluid would be critically increased [12]. Many MR dampers and MREAs filled with MR fluids have been studied [13–16]. Nguyen *et al* designed a linear stroke adaptive MREA and tested the performance under intense impact conditions [6, 17]. The maximum piston velocity was up to 8 m s^{-1} and the maximum damping force reached 15 kN. Mao *et al* proposed an MR damper with bi-fold valves for shock mitigation and used a nonlinear model to study the behavior under high speed impact conditions [18, 19]. Wereley *et al* analyzed the shock mitigation capabilities of an MREA and established a semi-active shock isolation system based on the MR damper [20, 21]. An MR seat suspension model was also constructed for military vehicles [22]. Hu *et al* proposed a new method to design high-performance MR dampers and MR valves [23, 24]. They added MR elastomers on an MR fluid damper to improve the stiffness variability and damping variability. They also designed an MR damper with improved displacement differential self-induced ability. Sun *et al* added MR elastomerson an MR fluid damper to improve the stiffness variability and damping variability [25]. Among the above researches, the MR fluid was used as the damping medium [26, 27] because the MR effect on MR fluids is high and the response time is short. However, the sealing, settlement and durability problem in MR fluids have limited their practical applications. Moreover, Choi *et al* reported the temperature-dependent dynamic characteristics of a piezo-electric actuator

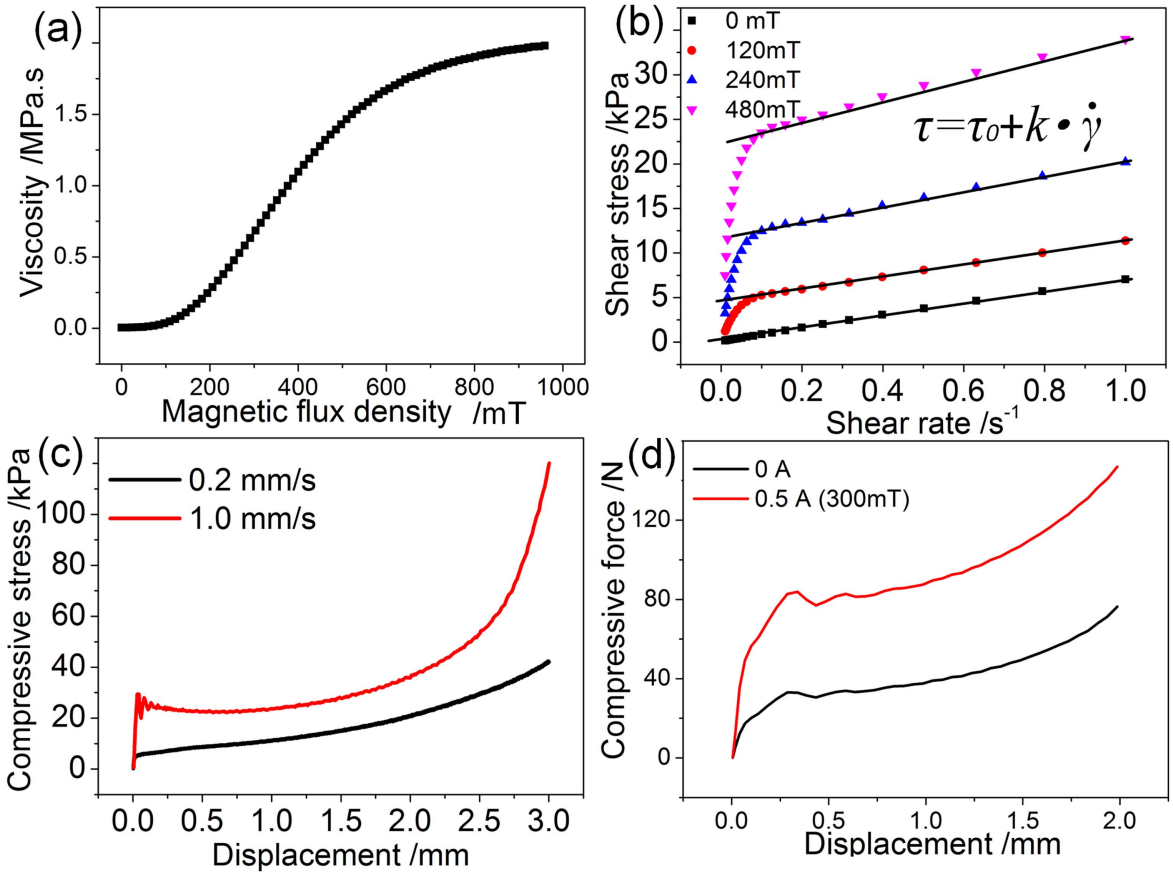

Figure 1. The mechanical properties of the MR gel (a). The shear viscosity of the MR gel under different magnetic fields, (b) the shear stress on the MR gels under different magnetic flux densities and different shear rates, (c) the compressive stress on the MR gel with different squeezing velocity under a squeeze mode and (d) the compressive force on the MR gel with different magnetic fields under a squeeze mode.

under high temperature. They found that both the strain and blocking force were decreased with increasing the temperature [28, 29].

The MR gels were composed of carbonyl iron particles and a polymer gel [30–33]. Due to the high viscosity of polymer gel, the MR gels had better stability than the MR fluids. Considering its high MR effect, MR gel was prospective in engineering applications such as MR vibration absorbers [34]. Unfortunately, few works have studied the performance of an MREA filled with MR gels. One of the most important parameters of an MREA is the maximum damping force. To improve the maximum damping force, increasing the viscosity of the damping medium is a direct way. Using MR gel as the damping medium could increase the damping force of an MREA and reduce the damping distance. On the one hand, the saturated magnetic field of an MR gel is large, thus the design of the electromagnet is complex. On the other hand, it is easy to generate a force pulse in an MREA filled with high viscose damping medium under an impact. How to utilize the whole damping range is important for shock mitigation. Therefore, designing an MREA with high damping force, short distance, and adjustable damping force is urgent.

This work reports a novel MREA in which an MR gel is used as the damping medium. To better control the damping force and make full use of the advantages of MR gel, the damping gap distance of the MREA was designed to be decreased as the piston was pressed down. The internal magnetic flux density distribution was also simulated and the magnetic field dependent performance was analyzed. Finally, the damping forces of the MREA under low speed compression and high speed impact were studied.

Experimental details

Test system

The rheological properties of MR gel were tested by a commercial rheometer Physica MCR301 (produced by Anton Paar GmbH, Austria) equipped with an electro-magnetic accessory MRD180. An electromechanical universal testing machine (Model 43, MTS System Corporation, China) was used to test the mechanical properties under compression. The buffer performance of the MREA was tested on a drop hammer test system (ZCJ1302-A, MTS System Corporation, China). The weight and height of the drop hammer were tunable and the acceleration signal of the hammer was recorded. During the test, the current input was controlled by a dc power supply (IT6724, Itech Electronics, Co., Ltd, China).

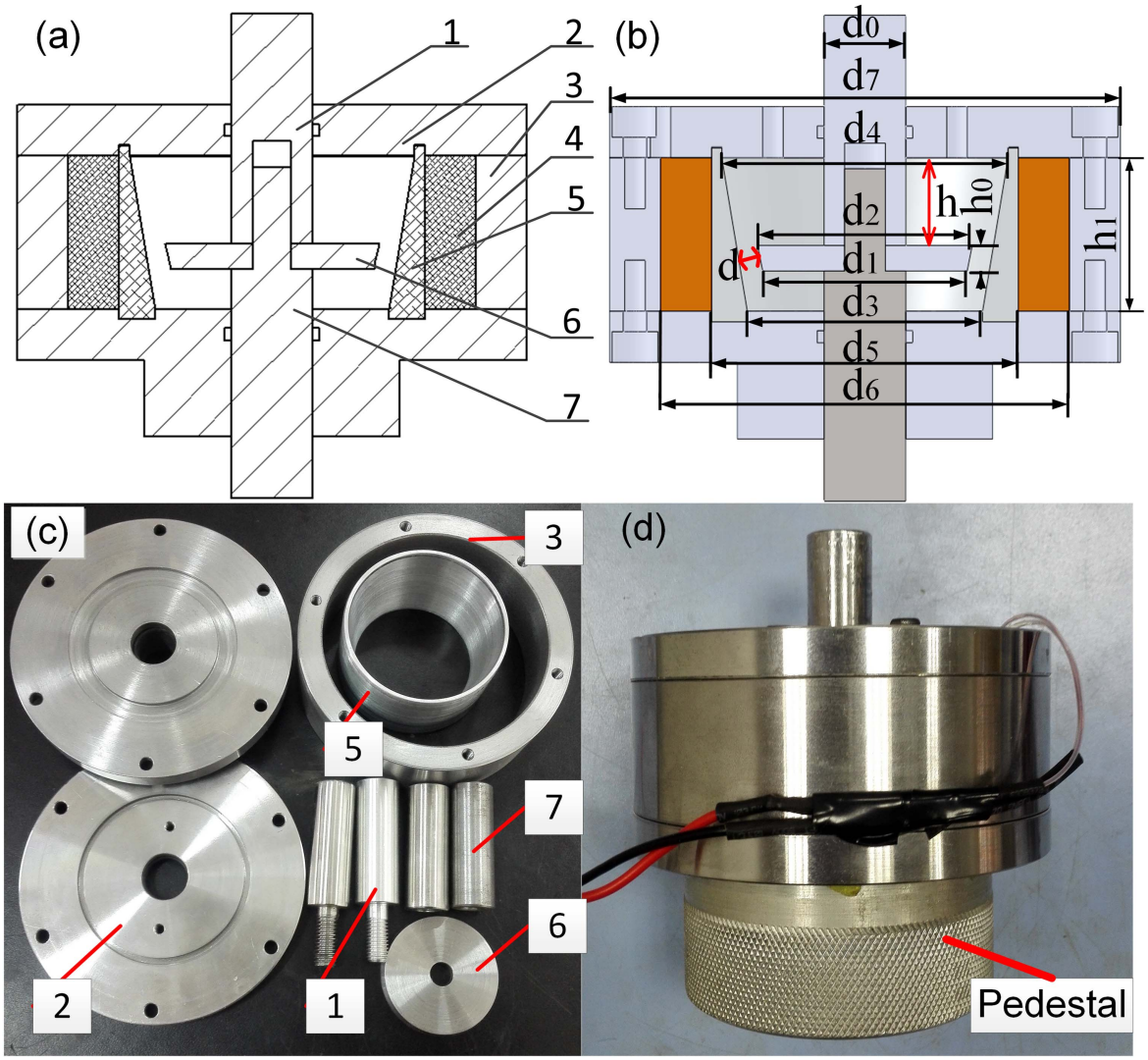

Figure 2. Schematic diagram, design parameters and photographs of the MREA with a tunable resistance gap: 1. Upper piston rod, 2. end cover, 3. coat, 4. exciting coil, 5. insulation lining, 6. piston, 7. nether piston rod.

Preparation and mechanical properties of MR gel

MR gel with 70 wt% carbonyl iron powders was prepared and used in the MREA. The materials used for the MR gel were: toluene diisocyanate (TDI, 2,4-TDI at ~80%, 2,6-TDI at ~20%, Tokyo Chemical Industry Co. Ltd, Japan), polypropylene glycol (PPG-1000, Sinopec Group Co. Ltd, China), 1,4-Butanediol (BDO, Sinopharm Chemical Reagent Co., Ltd, China), carbonyl iron powder (CIP, type CN, BASF Aktiengesellschaft, Germany) and 1-methyl-2-pyrrolidone (Sinopharm Chemical Reagent Co., Ltd, China). Firstly, TDI and PPG were added to a flask with the molar ratio 3:1 at 80 °C for 2 h. Their weights were calculated by the formula bellow:

$$\frac{m_{\mathrm{TDI}}/174 \cdot \mathrm{mol}^{-1}}{m_{\mathrm{PPG}}/1000 \cdot \mathrm{mol}^{-1}} = 3, \tag{1}$$

where m_{TDI} and m_{PPG} represent the weight of PPG and TDI, respectively. Later the temperature of the mixture was lowered to 60 °C and BDO was added into the reactor. The weight of the BDO was calculated by the formula bellow:

$$\frac{m_{\mathrm{TDI}}/174 \cdot \mathrm{mol}^{-1}}{\frac{m_{\mathrm{PPG}}}{1000} \cdot \mathrm{mol}^{-1} + \frac{m_{\mathrm{BDO}}}{90} \cdot \mathrm{mol}^{-1}} = 1.1\,, \tag{2}$$

Table 1. MREA design variables.

Parameter	Value
Diameter of the rod d_0	16 mm
Diameter of the bottom piston edge d_1	40 mm
Diameter of the top piston edge d_2	42 mm
Thickness of the piston h_0	5 mm
Thickness of the exciting coil h_1	30 mm
Inner diameter of the top insulation lining edge d_4	56 mm
Inner diameter of the bottom insulation lining edge d_3	44 mm
Diameter of the insulation lining d_5	60 mm
Diameter of the exciting coil d_6	80 mm
Diameter of the coat d_7	100 mm

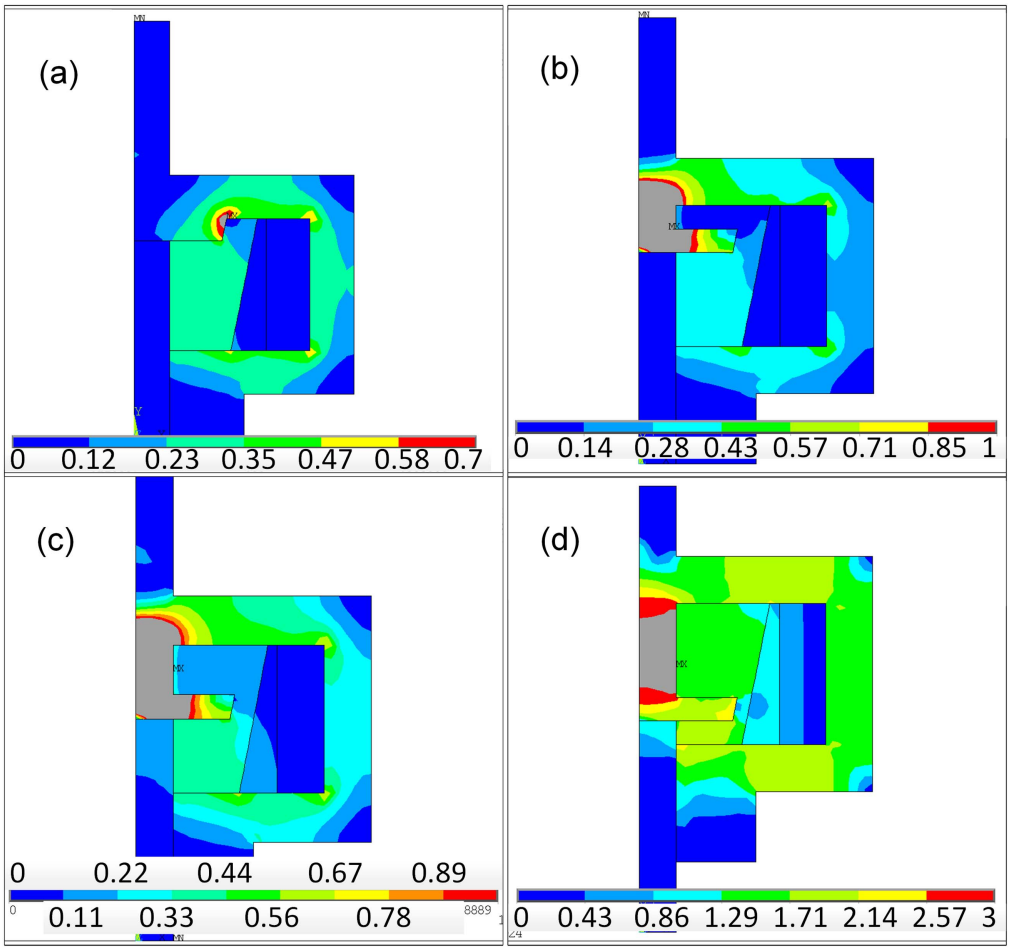

Figure 3. The magnetic flux density contour in the MREA with different piston positions. The displacement of the piston was 0 mm, 5 mm, 10 mm and 20 mm, respectively.

where m_{BDO} represents the weight of the BDO. 40 min later, 1-methyl-2-pyrrolidone was added into the mixture at a 10 wt% ratio. Once the polymer gel was synthesized, the CIPs were added under vigorously mixing before the temperature was cooled down.

Obviously, the shear viscosity of the MR gel was highly dependent on the magnetic field, so the shear stress was changed by a large range by applying the magnetic field (figure 1(b)). The shear stress increased with the increasing of shear rate and it could be expressed as

$$\tau = \tau_0 + k\dot{\gamma} \tag{3}$$

In equation (3), τ is the shear stress, τ_0 is the yield stress and is dependent on the magnetic field and $\tau_0 = 22$ kPa for the MR gel under a 480 mT magnetic field. $\dot{\gamma}$ represents the shear rate and k is the coefficient to be determined. The mechanical properties of MR gel under a squeeze mode were also tested. The initial diameter of the sample was 20 mm and the initial height was 6 mm. There was a fast increase in the compressive force with decreasing the gap distance and then the sample was yielded. After a steady increase, the compressing force increased rapidly. So, the compression process can be divided into three parts. When the strain was smaller than 7%, the compressive force rapidly increased and the sample began to yield. After that, the compressive force increased slowly until the diameter–height ratio reached about 5, and the compressive stress quickly increased. The compressive stress was highly dependent on the magnetic field (figure 1(c)) and the compressive rate also had a strengthening influence on the compressing force (figure 1(d)).

Design of the MREA

Structure analysis of the MREA

The structure of the MREA is shown in figure 2. The basic components include: two piston rods, a piston, an insulation lining, an exciting coil, two end covers and a coat. MR gel was filled into the cavity between the insulation lining, and the end covers and an exciting coil was wrapped on the insulation lining. Figure 2(b) shows the parameters of the components and table 1 lists the values. The side of the piston was a slope and it was parallel to the inner face of the insulation lining, so the gap distance d decreased as the piston was pressed down. The maximum and minimum gap distance between the piston and the insulation lining were 7 mm and 2 mm, respectively. The equation between the gap distance d

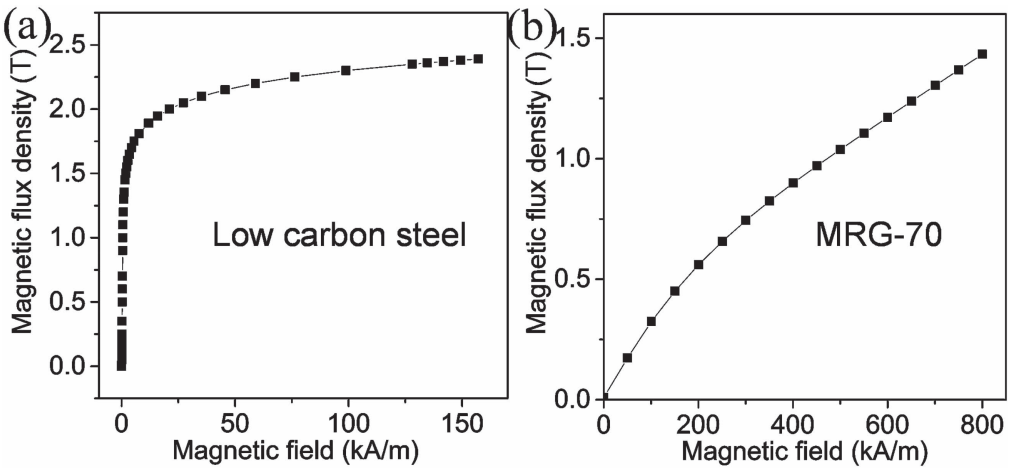

Figure 4. B-H curves of low carbon steel (a) and MRG with 70 wt% CIPs (b).

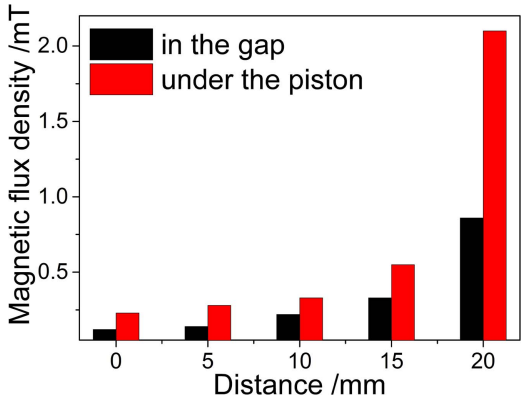

Figure 5. The magnetic flux density in the gap and under the piston with different piston displacement.

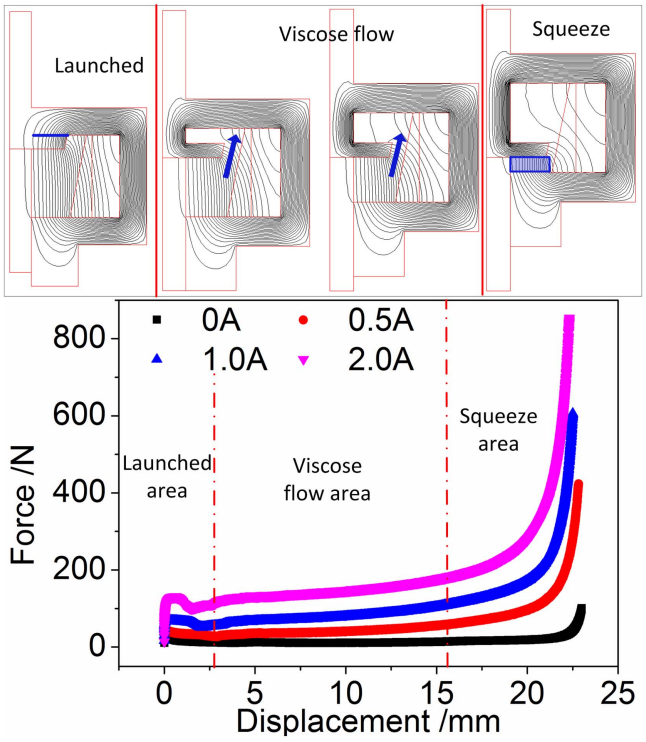

Figure 6. The damping force and distribution of the magnetic flux lines of the MREA as the piston was pressed down.

and the piston displacement h was $d = 7 - h/5$. With the piston moving down, the MR gel under the piston was squeezed and flowed to space above the piston by the gap. The damping force was the sum of the shear force (worked on the side of the piston) and the normal force (on the under-surface of the piston), thus the mechanical properties of MR gel under both a shear mode and squeeze mode had a big influence on the behavior of the MREA. When a constant direct current was applied in the exciting coil, a closed loop of magnetic circuits would be generated in the coat, the end covers, the upper piston rod, the piston, the resistance gap and the space between the piston and the bottom end covers. The end covers, the upper piston rod and the coat were made from No. 10 steel with high relative permeability and the nether piston rod was made from stainless steel with low relative permeability. The magnetic flux density in the gap changed with the piston position and this characteristic also helped adjust the energy dissipation process.

Simulation analysis of the magnetic field in the MREA

Since the mechanical properties of the MR gel were sensitive to a magnetic field, the inner magnetic flux density was simulated using ANSYS software. Figure 3 shows the magnetic flux density contour in an axisymmetric 2D model of the MREA. The upper piston rod, end cover, coat and piston were made from low carbon steel whose permeability was defined by the B-H curve in figure 4. The permeability of the MRG gel was also defined by the B-H curve. The nether piston rod was made from stainless steel, the exciting coil is copper and the insulation lining is aluminum with a relative permeability of 1. The number of coil turns was 1100 and the current was set as 2 A. Obviously, the magnetic flux density both under the piston and at the gap increased with the piston moving down, which meant the resistance force would increase if the compression velocity of the piston was constant

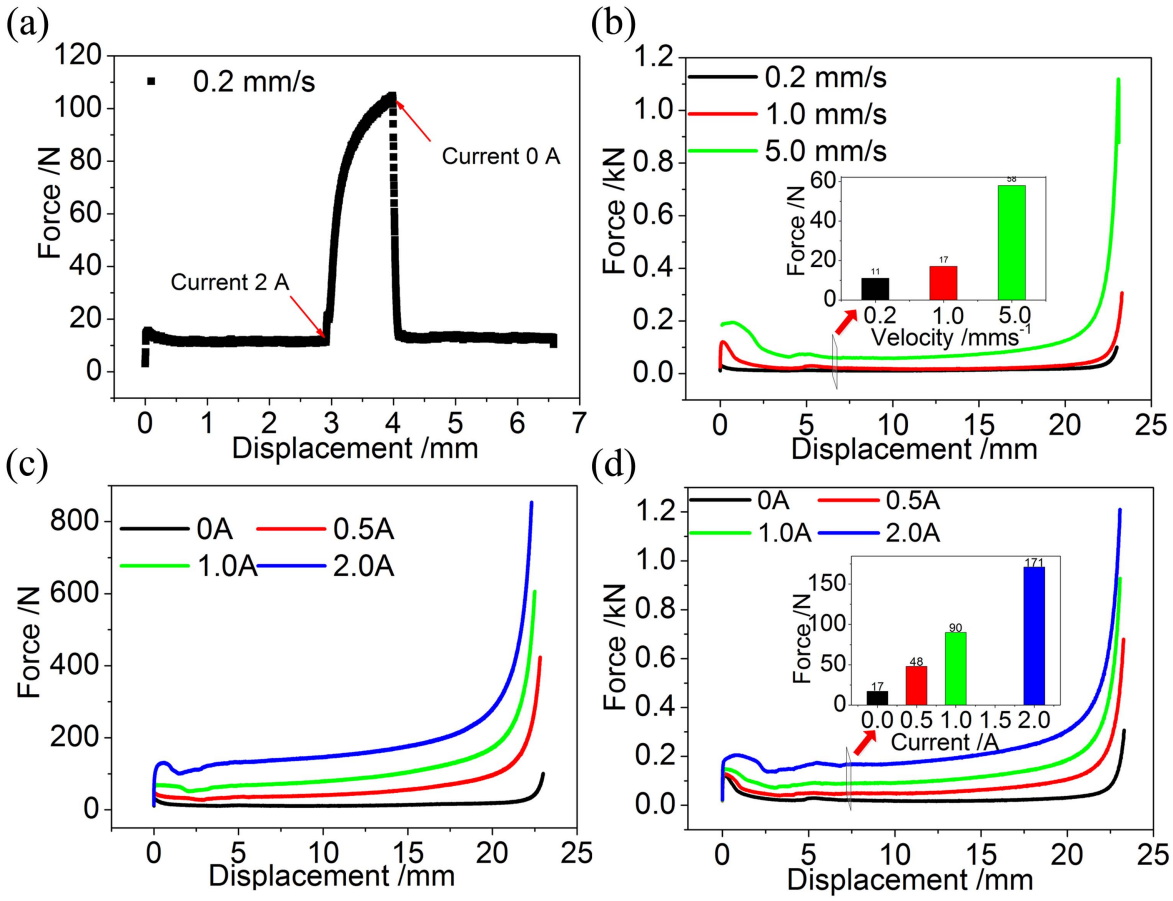

Figure 7. Resistance force of the MREA under different current and different compression velocity, (a) with a changing current, (b) under different compression velocity without current, (c) with different currents and a 0.2 mm s^{-1} compression velocity and (d) with different currents and a 1.0 mm s^{-1} compression velocity.

(figure 5). It is useful for energy absorbing especially for shock mitigation under a shock. With the piston moving down, the magnetic flux density in the gap increased from 120–860 mT. Generally, under a shock pulse, the velocity at the moment of contact was high and the resistance force was large because the shear force increased with the increasing of shear rate. To avoid the force pulse, the gap distance of the proposed MREA decreased as the piston was pressed down. So the shear rate was low at the moment of contact and gradually increased with the piston moving down. After the initial contact, the shock velocity was slowed down and the gap distance decreased to generate a relatively large force. At this time, if there was a current applied to the exciting coil, the magnetic flux density in the gap would increase with the piston moving down. The viscosity of the MR gel increased which further helped mitigate the impact. So, the proposed design can adjust the energy absorbing process and improve the utilization of the whole stroke.

Test results and discussion

Low velocity compression test

The low velocity compression test was carried out by a Modulab material test system. A pedestal was fixed on the end cover to support the MREA. A dc power was used to control the current in the exciting coil of the MREA. As shown in figure 6, the energy absorption process can be divided into three parts. When the displacement was less than 3 mm, there was an abrupt increase in the resistance force because of the mechanical friction and the yield of the MR gel. This area was named the launched area. After that, the compressive force increased gradually as the piston was pressed down under a constant velocity. The resistance force was mainly caused by the viscose flow of the MR gel in the gap. With the piston moving down, the gap distance d decreased and the shear rate increased, so the viscose force increased. In addition, when there was a current in the exciting coil, the magnetic field was presented in the resistance gap. The simulation results demonstrated that the magnetic field was basically perpendicular to the gap. The magnetic flux density in the gap increased with the piston moving down; thus, it further improved the force. With further increasing of the displacement (more than 17 mm), the MR gel under the piston was squeezed and the resistance force increased rapidly. The magnetic flux lines under the piston were also vertical to the undersurface of the piston, which was useful for the MR gel to produce a large normal force with the current input. The rapidly increased force could avoid the contact of the piston and the end cover. In other

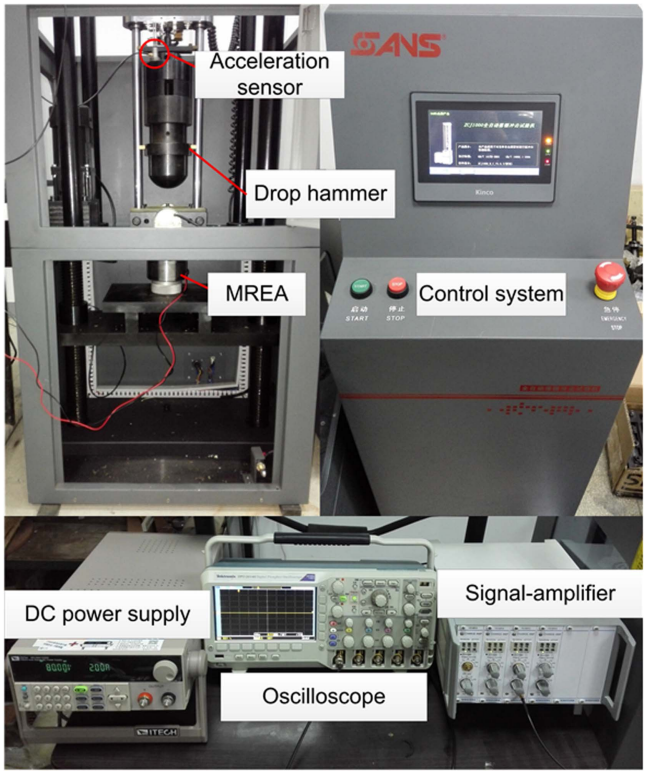

Figure 8. Drop hammer test rig of the MREA.

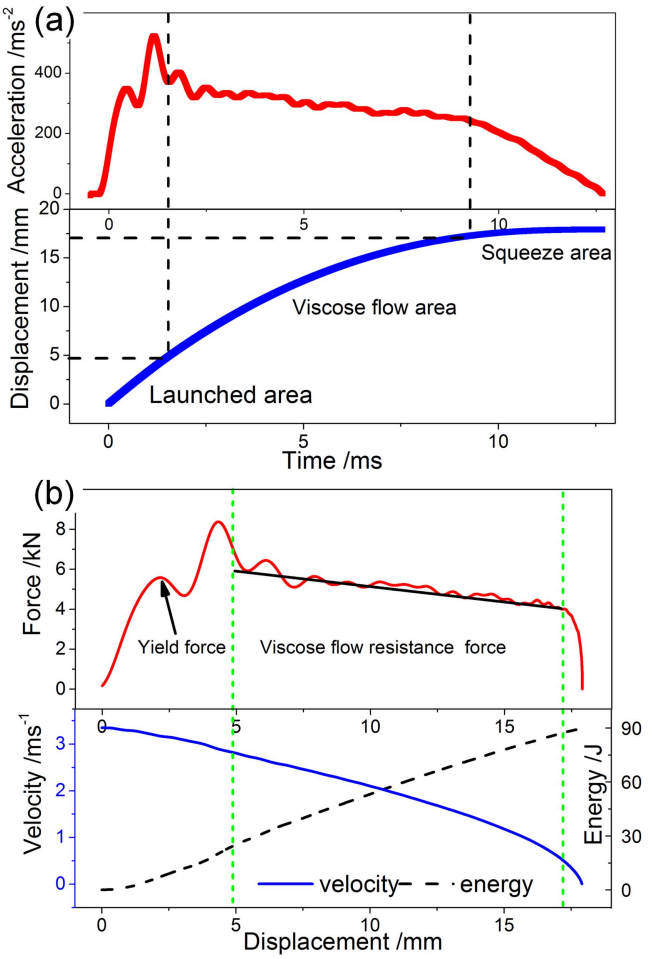

Figure 9. The load-stroke profile of MREA. The weight of the drop hammer was 16 kg and the height was 80 cm.

words, the resistance force increased as the piston was pressed down during the entire process. When the compression velocity was constant, it was useful to counteract the pulse force caused by the impact. The resistance force could also be changed in a large range by applying a current to the exciting coil (figures 7(a)–(d)) and it was highly dependent on the compression velocity (figure 7(b)). Here, the compressive force increased from 17–171 N with the current increasing from 0–2 A.

Drop hammer test of MREA

The drop hammer test system was built to evaluate the shock mitigation capabilities of the MREA (figure 8). The MREA was fixed on the substrate of the drop hammer test system and the current input was controlled by dc power. During the drop hammer testing, an acceleration sensor was fixed on the drop hammer and the signal was converted by a signal-amplifier and recorded with an oscilloscope. The acceleration signal of the hammer was recorded during the impact. The force on the hammer could be calculated by Newton's second law. The hammer struck the piston rod then the force on the piston rod was equal to the force on the hammer. The change in the velocity was calculated by integrating the acceleration signal and the displacement was calculated by integrating the velocity. As shown in figure 9, there was an abrupt increase in the impact force at the moment of contact. The resistance force decreased after the abrupt increase because the MR gel yielded and then rebounded in the MREA. At the displacement of 5 mm, the force reached the maximum but did not drop rapidly. Until the displacement reached16 mm, the resistance decreased rapidly. So, the whole stroke of the proposed MREA was thoroughly used to mitigate the shock and avoid the force pulse. Due to the friction between the hammer and the track, the maximum speed of the piston was less than the free fall speed of the hammer. The velocity of the piston was reduced from 3.4–0 m s^{-1} in 13 ms with a 17 mm distance. Combining equation (3), we can get the viscous resistance force:

$$F = s\tau = ks\dot{\gamma}, \tag{4}$$

where F represents the viscous resistance force and s is the side area of the piston and $\dot{\gamma}$ represents the shear rate. In the viscose flow area, the velocity reduced from 2.8–0.8 m s^{-1} (decreased 70%) but the force decreased from 6–4 kN (decreased 33%). That was because the gap distance d also reduced with the decreasing of the velocity, which slowed down the decrease of the shear rate. At the last 2 mm, the piston was close to the end cover and the velocity of the piston dropped rapidly. The absorbed energy evenly rose which met the design expectations.

To further test the shock mitigation capabilities of the MREA, drop hammers with different weights were dropped from different heights. The tendency of the force curves with

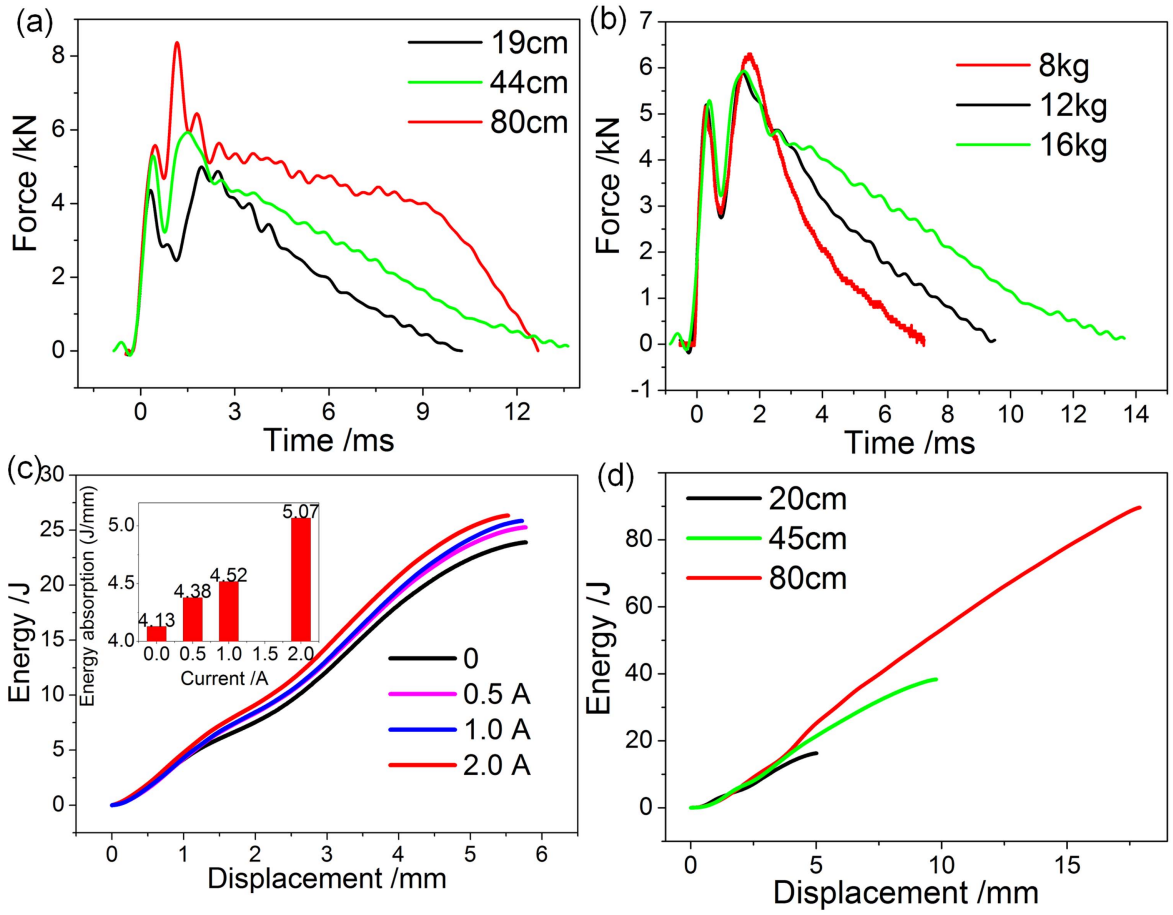

Figure 10. The resistance force and energy absorption of the MREA with different drop heights, different drop hammer weights and different current inputs: (a) and (d) different drop height, 8 kg drop mass, 0 A current input, (b) different drop mass weight, 44 cm drop height, 0 A current input, (c) different current input, 8 kg drop mass, 44 cm drop height.

different drop heights and drop mass weights were similar. For the experiments with different drop heights, the maximum force increased with increasing of the drop height. The velocity with higher drop height was larger and the viscose force was bigger, then the maximum force increased. For tests with different drop mass weights, the velocities of the drop hammers were the same, so the front part of the force curves was roughly coincident (figure 10(b)). Here, the shock energy with heavier drop mass was higher. The energy absorbed at the first 2 ms was the same, so the force later in the process was higher with heavier drop mass. The proposed MREA can mitigate the impact of different drop mass weights without increasing the maximum force, which is useful for practical application. For impacts with different drop heights, the maximum force was not proportional to the height. Much more energy was consumed in the latter part of the absorption (figure 10(a)). Figure 10(c) shows the energy absorption during the test with different current inputs. The energy absorption ratio increased from 4.13 J mm^{-1} with 0 A current to 5.07 J mm^{-1} with 2 A current. The energy absorption ratio increased by about 23%. The energy absorption with different displacements was also calculated. The curves were basically straight lines which meant the energy absorption was uniform for the whole stroke.

Conclusion

In this work, an MREA based on MR gels was designed and tested. The gap distance of the proposed MREA decreased as the piston was pressed down. The calculated magnetic flux density distribution in the MREA showed the magnetic flux density increased with decreasing of the gap distance. The proposed design could lead to the increase of damping force under a constant speed compression. The damping force of the MREA under both low velocity compression and high speed impact was tested. The compression process can be divided into three parts. In the drop hammer test, the damping force did not increase with increasing weight of the drop mass and the velocity of the piston could be reduced from 3.4 m s^{-1} to 0 m s^{-1} in 13 ms. The maximum damping force in the test reached about 8 kN when the drop height was 80 cm (3.4 m s^{-1} piston velocity). The magnetic field intensity of the eletromagnet could also adjust the damping process and the energy absorption ratio increased from 4.13 J mm^{-1} with 0 A current to 5.07 J mm^{-1} with 2 A current (23%). The energy absorption ratio was uniform for the whole damping process, which meant that an MR gel could be used in an MREA for shock mitigation.

Acknowledgments

This work was supported by the National Natural Science Foundation of China (Grant Nos. 11572309, 11572310), the Fundamental Research Funds for the Central Universities (WK2480000002) and the Strategic Priority Research Program of the Chinese Academy of Sciences (Grant No. XDB22040502). This study was also supported by the Collaborative Innovation Center of Suzhou Nano Science and Technology.

References

[1] Alghamdi A A A 2001 Collapsible impact energy absorbers: an overview *Thin Wall Struct.* **39** 189–213
[2] Moreno C, Williams T, Beaumont R, Hughes D J and Dashwood R 2016 Testing, simulation and evaluation of a novel hybrid energy absorber *Int. J. Impact Eng.* **93** 11–27
[3] Dogruer U, Gordaninejad F and Evrensel C A 2008 A new magneto-rheological fluid damper for high-mobility multi-purpose wheeled vehicle (HMMWV) *J. Intell. Mater. Syst. Struct.* **19** 641–50
[4] Facey W B, Rosenfeld N C, Choi Y T, Wereley N M, Choi S B and Chen P 2005 Design and testing of a compact magnetorheological damper for high impulsive loads *Int. J. Mod. Phys.* B **19** 1549–55
[5] Mao M, Hu W, Choi Y T, Wereley N M, Browne A L and Ulicny J 2014 Experimental validation of a magnetorheological energy absorber design analysis *J. Intell. Mater. Syst. Struct.* **25** 352–63
[6] Nguyen Q H, Nguyen N D and Choi S B 2015 Design and evaluation of a novel magnetorheological brake with coils placed on the side housings *Smart Mater. Struct.* **24** 047001
[7] Singh H J and Wereley N M 2013 Adaptive magnetorheological shock isolation mounts for drop-induced impacts *Smart Mater. Struct.* **22** 122001
[8] Choi S B, Li W H, Yu M, Du H P, Fu J and Do P X 2016 State of the art of control schemes for smart systems featuring magneto-rheological materials *Smart Mater. Struct.* **25** 043001
[9] Li Z X and Xu L H 2005 Performance tests and hysteresis model of MRF-04K damper *J. Struct. Eng.* **131** 1303–6
[10] Xing Z W, Yu M, Sun S S, Fu J and Li W H 2016 A hybrid magnetorheological elastomer-fluid (MRE-F) isolation mount: development and experimental validation *Smart Mater. Struct.* **25** 015026
[11] Gong X L, Ruan X H, Xuan S H, Yan Q F and Deng H X 2014 Magnetorheological damper working in squeeze mode *Adv. Mech. Eng.* 410158
[12] de Vicente J, Klingenberg D J and Hidalgo-Alvarez R 2011 Magnetorheological fluids: a review *Soft Matter* **7** 3701–10
[13] Bai X X, Chen P and Qian L J 2015 Principle and validation of modified hysteretic models for magnetorheological dampers *Smart Mater. Struct.* **24** 085014
[14] Jiang N, Sun S S, Ouyang Y M, Xu M, Li W H and Zhang S W 2016 A highly adaptive magnetorheological fluid robotic leg for efficient terrestrial locomotion *Smart Mater. Struct.* **25** 095019
[15] Sun S S, Ning D H, Yang J, Du H, Zhang S W and Li W H 2016 A seat suspension with a rotary magnetorheological damper for heavy duty vehicles *Smart Mater. Struct.* **25** 105032
[16] Tu J W, Liu J, Qu W L, Zhou Q, Cheng H B and Cheng X D 2011 Design and fabrication of 500 kN large-scale MR damper *J. Intell. Mater. Syst. Struct.* **22** 475–87
[17] Nguyen Q H and Choi S B 2009 Optimal design of MR shock absorber and application to vehicle suspension *Smart Mater. Struct.* **18** 035012
[18] Mao M, Hu W, Choi Y T, Wereley N M, Browne A L, Ulicny J and Johnson N 2013 Nonlinear modeling of magnetorheological energy absorbers under impact conditions *Smart Mater. Struct.* **22** 115015
[19] Mao M, Hu W, Choi Y T and Wereley N M 2007 A magnetorheological damper with bifold valves for shock and vibration mitigation *J. Intell. Mater. Syst. Struct.* **18** 1227–32
[20] Wereley N M, Choi Y T and Singh H J 2011 Adaptive energy absorbers for drop-induced shock mitigation *J. Intell. Mater. Syst. Struct.* **22** 515–9
[21] Choi Y T and Wereley N M 2008 Shock isolation systems using magnetorheological dampers *J. Vib. Acoust.* **130** 024503
[22] Choi Y T and Wereley N M 2005 Mitigation of biodynamic response to vibratory and blast-induced shock loads using magnetorheological seat suspensions *Proc. Inst. Mech. Eng.* **219** 741–53
[23] Hu G L, Long M, Yu L F and Li W H 2014 Design and performance evaluation of a novel magnetorheological valve with a tunable resistance gap *Smart Mater. Struct.* **23** 127001
[24] Hu G L, Zhou W and Li W H 2015 A new magnetorheological damper with improved displacement differential self-induced ability *Smart Mater. Struct.* **24** 087001
[25] Sun S S, Yang J, Li W H, Deng H X, Du H P and Alici G 2015 Development of a novel variable stiffness and damping magnetorheological fluid damper *Smart Mater. Struct.* **24** 085021
[26] Choi S B, Seong M S and Ha S H 2009 Vibration control of an MR vehicle suspension system considering both hysteretic behavior and parameter variation *Smart Mater. Struct.* **18** 125010
[27] Singh H J and Wereley N M 2014 Optimal control of gun recoil in direct fire using magnetorheological absorbers *Smart Mater. Struct.* **23** 055009
[28] Han C, Jeon J, Chung J U and Choi S B 2015 Dynamic characteristics and control capability of a piezostack actuator at high temperatures: experimental investigation *Smart Mater. Struct.* **24** 057002
[29] Han Y M, Han C, Kim W H, Seong H Y and Choi S B 2016 Control performances of a piezoactuator direct drive valve system at high temperatures with thermal insulation *Smart Mater. Struct.* **25** 097003
[30] An H N, Picken S J and Mendes E 2012 Nonlinear rheological study of magneto responsive soft gels *Polymer* **53** 4164–70
[31] Yang P G, Yu M, Luo H P, Fu J, Qu H and Xie Y P 2017 Improved rheological properties of dimorphic magnetorheological gels based on flower-like carbonyl iron particles *Appl. Surf. Sci.* **416** 772–80
[32] Ju B X, Yu M, Fu J, Zheng X and Liu S Z 2013 Magnetic Field-Dependent Normal Force of Magnetorheological Gel *Ind. Eng. Chem. Res.* **52** 11583–9
[33] Fuchs A, Xin M, Gordaninejad F, Wang X, Hitchcock G H, Gecol H, Evrensel C and Korol G 2004 Development and characterization of hydrocarbon polyol polyurethane and silicone magnetorheological polymeric gels *J. Appl. Polym. Sci.* **92** 1176–82
[34] Kim H K, Kim H S and Kim Y K 2017 Stiffness control of magnetorheological gels for adaptive tunable vibration absorber *Smart Mater. Struct.* **26** 015016